Available online at www.sciencedirect.com

ScienceDirect

www.elsevier.com/locate/jes

JES JOURNAL OF ENVIRONMENTAL SCIENCES

www.jesc.ac.cn

Research Article

Evaluating coarse PM composition and sources based on bulk and molecular speciation of $PM_{2.5}$ and PM_{10} in Nanjing, East China

Wangnan Cui[1], *Zishu Wang*[2], *Wei Feng*[1], *Chao Qin*[3], *Hong Liao*[1], *Yuhang Wang*[4], *Mingjie Xie*[1,*]

[1] *Collaborative Innovation Center of Atmospheric Environment and Equipment Technology, Jiangsu Key Laboratory of Atmospheric Environment Monitoring and Pollution Control, School of Environmental Science and Engineering, Nanjing University of Information Science & Technology, Nanjing 210044, China*

[2] *Nuist Reading Academy, Nanjing University of Information Science & Technology, Nanjing 210044, China*

[3] *State Environmental Protection Key Laboratory of Monitoring and Analysis for Organic Pollutants in Surface Water, Jiangsu Environmental Monitoring Center, Nanjing 210036, China*

[4] *School of Earth and Atmospheric Sciences, Georgia Institute of Technology, Atlanta GA 30332, United States*

ARTICLE INFO

Article history:
Received 29 December 2023
Revised 16 April 2024
Accepted 22 April 2024
Available online 28 April 2024

Keywords:
Coarse particle
Bulk species
Organic molecular marker
Light absorption
Source apportionment

ABSTRACT

To understand the differences in the composition and sources of $PM_{2.5}$ and PM_{10} caused by coarse particles, integrated $PM_{2.5}$ and PM_{10} samples were synchronously collected in Nanjing, East China, in summer 2020 and winter 2020/2021. Bulk and molecular speciation and light absorption measurements of aerosol extracts were performed, followed by positive matrix factorization (PMF) based on the $PM_{2.5}$ and PM_{10} data sets, respectively. The difference in average concentrations of total bulk species between $PM_{2.5}$ and PM_{10} was mainly caused by the distribution of considerable NO_3^-, SO_4^{2-}, Ca^{2+}, and organic carbon (OC) in coarse particles. Coarse PM influenced by abrasion products from tire wear and leaves contributed about half of the low-volatility *n*-alkanes in summer. The contribution of coarse PM to biomass burning tracers and water-soluble OC increased in winter when biomass combustion was excessively active. More than 70% of sugar polyols were attributable to coarse PM in summer, and biomass burning could be an important source in winter. The light-absorbing organic chromophores were almost entirely associated with $PM_{2.5}$, but water-soluble organic carbon (WSOC) exhibited stronger light absorption in PM_{10} extracts than in $PM_{2.5}$ extracts possibly due to the influence of coarse PM on pH. PMF analysis indicated that biomass burning, aqueous-phase reactions, and processed dust were the main contributors of organic matter and its light absorption in winter. Biogenic primary and secondary sources made

* Corresponding author.
E-mail: mingjie.xie@nuist.edu.cn (M. Xie).

https://doi.org/10.1016/j.jes.2024.04.038

discernable contributions only in summer. The differences between $PM_{2.5}$ and PM_{10} were likely attributed to mixing of crustal dust, combustion particles, and surface reactions.

Introduction

Chinese cities have long suffered from air pollution problems caused by particulate matter (PM) with an aerodynamic diameter ≤ 2.5 μm ($PM_{2.5}$) and respirable suspended particles (PM_{10}). Numerous studies have been conducted to reveal the pollution levels, chemical composition, sources, and climate and health impacts of fine PM in Chinese cities (Cao et al., 2012; Huang et al., 2017; Tao et al., 2017; Zhang et al., 2019; Liu et al., 2020; Hong et al., 2020). Evidence shows that the fine PM can be well explained by NO_3^-, SO_4^{2-}, NH_4^+, organic carbon (OC), and elemental carbon (EC); NO_3^- became the most abundant species in $PM_{2.5}$ instead of SO_4^{2-} based on their annual average concentrations in Nanjing since 2017 (Yu et al., 2020; Xie et al., 2022b). OC and its light absorption, a measurement proxy of brown carbon (BrC), in $PM_{2.5}$ were majorly contributed by biomass and fossil fuel combustion and secondary formations (Yuan et al., 2020; Feng et al., 2023b). However, a significant fraction of coarse PM in the size range of 2.5–10 μm is still unknown, and the organic components of coarse PM have been less studied.

In both Nanjing and Hong Kong, bulk components (inorganic ions, OC, and EC) and trace elements only accounted for only ~ 75% of the coarse PM (Xie et al., 2022a; Wong et al., 2022). Ecotoxicological studies have shown that primary biological aerosols (e.g., microorganisms) mainly associated with coarse PM can cause infectious diseases, toxic reactions, and immunostimulatory signals upon skin contact, ingestion, and inhalation (Shiraiwa et al., 2017). Based on size-resolved PM sampling and measurements, the majority of bulk species in coarse PM have been apportioned to a variety of dust sources (e.g., mineral dust and road dust; Tian et al., 2016; Xie et al., 2022a), and aerosol extract absorption has been found to be enriched in the accumulation mode (Liu et al., 2013; Wu et al., 2020a). Due to the low PM loading of individual size ranges in coarse mode and positive sampling artifacts of semi-volatile organics, the organic speciation and BrC absorption measurement for coarse PM and subsequent source apportionment can be subject to substantial uncertainties (Xie et al., 2022a; Feng et al., 2023a). To a large extent, understanding the environmental behavior of atmospheric PM depends on how well it is characterized.

In this study, $PM_{2.5}$ and PM_{10} samples were collected simultaneously during the summer of 2020 and the winter of 2020 to 2021 at a suburban site in northern Nanjing, China. Each sample was analyzed for bulk components, non-polar and polar organic molecular markers (OMMs) with different volatility and/or sources, and light absorption of aerosol extracts in water and methanol. Positive matrix factorization (PMF) was applied to identify and quantify the sources of the measured PM components and aerosol extract absorption based on the speciation data. Measurement and source apportionment results of $PM_{2.5}$ and PM_{10} were compared to evaluate the differences, which will benefit the development of PM_{10} control measures to reduce the health and climate impacts associated with coarse PM.

1. Methods

1.1. *Sampling*

$PM_{2.5}$ and PM_{10} samples were collected on the rooftop of a seven-story library building (~ 22 m high) at Nanjing University of Information Science and Technology (NUIST, 32.21° N, 118.71° E). Two identical mid-volume samplers (Laoying 2030, Lonying Environmental, China) equipped with 2.5 μm and 10 μm cut-point impactors, respectively, were used to simultaneously collect $PM_{2.5}$ and PM_{10} at a flow rate of 100 L/min. After passing through the impactor, the PM in the air stream was filtered through a pre-baked (550°C, 4 hr) quartz fiber filter (Ø = 90 mm, MK360, Munktell, Sweden). Sampling was conducted from 05/31/2020 to 09/07/2020 (summer) and from 12/01/2020 to 01/25/2021 (winter) during the hours 8:00–19:00 (daytime) and 20:00–7:00 (the next day, nighttime). A total of 147 pairs of filer samples were collected in summer and 93 pairs in winter. Field blanks were collected on every 5th sample day to correct for contamination. To evaluate the impact of differences between samplers on the comparison of $PM_{2.5}$ and PM_{10} measurements, the two samplers were configured to collect PM of the same size simultaneously in June 2020 ($PM_{2.5}$, 8 pairs; PM_{10}, 8 pairs). See Appendix A Table S1 in the Supplementary data for more details on sampling dates and times. Prior to chemical analysis, all filter samples were stored at –20°C in a freezer.

1.2. *Measurements of aerosol components and extract absorption*

The methods for chemical speciation and light-absorption measurement of aerosol extracts were developed and validated in our previous studies (Yang et al., 2021; Gou et al., 2021; Qin et al., 2021; Xie et al., 2022c). Inorganic ions in the water extracts, including NH_4^+, SO_4^{2-}, NO_3^-, Cl^-, Ca^{2+}, Mg^{2+}, and Na^+, were determined by ion chromatography (930 Compact IC, Metrohm IG, Switzerland; ICS2000, Dionex, United States). Data for Na^+, Cl^-, and Mg^{2+} were omitted due to unreliable results. Water-soluble OC (WSOC) and water-soluble total nitrogen (WSTN) in the same extracts were analyzed using a total organic carbon analyzer with a TN model (TOC-L/TNM-l, Shimadzu, Japan). WSON was calculated by subtracting inorganic nitrogen (NH_4^+-N + NO_3^--N) from WSTN (Yang et al., 2021). OC and EC in each filter sample were measured using a thermo-optical carbon analyzer (DRI, 2001A, Atmoslytic, United States) following the IMPROVE-A protocol.

After the addition of deuterated PAHs to filter samples as internal standards (IS), non-polar and polar OMMs were ex-

tracted in pure dichloromethane (DCM) and a methanol-DCM mixture (vol:vol, 1:1), respectively. The DCM extracts were filtered and concentrated to ~ 200 μL before analyzing the non-polar OMM using an Agilent 7890B gas chromatograph (GC) coupled to an Agilent 5977B mass spectrometer (MS). Prior to GC–MS determination, polar OMMs (polyols and carboxylic acids) were converted to trimethylsilyl ethers and esters by N, O-bis(trimethylsilyl)trifluoroacetamide (BSTFA) derivatization. Mass quantification of all OMMs was performed by the IS method with six-point calibration curves. The full names, abbreviations, molecular weights (MWs), and reference standards of the target OMMs are listed in Appendix A Table S2. Further details on sample extraction and instrumental analysis can be found in Appendix A Text S1.

The light absorbance of water ($A_{\lambda,w}$) and methanol ($A_{\lambda,m}$) extracts of each sample was retrieved using a UV/Vis spectrometer (UV-1900, Shimadzu, Japan) in the range of 200 to 900 nm. The light absorption coefficients ($Abs_{\lambda,w}$ and $Abs_{\lambda,m}$, Mm^{-1}) were calculated to represent the light absorption of WSOC and methanol-extractable OC (MEOC). Mass absorption efficiency ($MAE_{\lambda,w}$ and $MAE_{\lambda,m}$, m^2/gC), a measure of light absorption per unit mass of chromophores, was determined by normalizing $Abs_{\lambda,w}$ and $Abs_{\lambda,m}$ with the mass concentrations of WSOC and MEOC. Here, MEOC concentrations ($\mu g/m^3$) were estimated to be 82.4% × OC (Xie et al., 2022c). Because the values of $A_{\lambda,w}$ and $A_{\lambda,m}$ at $\lambda > 400$ nm were close to 0 and highly uncertain, the solution absorption Ångström exponent (Å), typically determined by regression of lg (Abs_λ) to lg (λ) at 300–550 nm, was not calculated. To be consistent with previous studies, Abs_λ and MAE_λ values were reported and discussed at 365 nm. Further details on sample extraction and Abs_λ and MAE_λ calculations are provided in Appendix A Text S2.

1.3. *Source apportionment*

In this work, PMF version 5.0 was used as the primary tool for source apportionment. The solution is to minimize the sum of squared and scaled residuals when assigning measured data to specific source-related factors. Details on data preparation and factor number determination can be found in Appendix A Text S3. Candidate input species were selected based on the proportion of valid measurements, signal-to-noise ratio, physical meaningfulness of PMF base-case solutions, and volatility of non-polar OMMs. The resulting $PM_{2.5}$ and PM_{10} data sets consisted of 225 and 223 observations of 43 species, respectively (Appendix A Table S2). The final factor number was determined primarily based on the interpretability of each base-case solution. Robustness assessment results and Q/Q_{exp} values for PMF analysis with different factor numbers (4–10) are also considered and summarized in Appendix A Tables S3 and S4.

2. Results and discussion

2.1. *Overview of the measurement data*

The mean values and ranges of bulk components, OMM groups, and Abs_{365} and MAE_{365} of WSOC and MEOC in $PM_{2.5}$ and PM_{10} are summarized in Appendix A Table S5. Appendix A Tables S6 and S7 show the average concentrations and ranges of individual OMMs. Wintertime WSTN and inorganic nitrogen (NH_4^+-N + NO_3^--N) in $PM_{2.5}$ were strongly correlated ($r = 1.00$) and showed no significant differences (Student's t-test, $p = 0.32$), indicating that $PM_{2.5}$-associated WSTN in winter is almost exclusively in the form of NH_4^+ and NO_3^-. Therefore, winter WSON concentrations in $PM_{2.5}$ were not reported. Appendix A Figs. S1–S6 exhibit the time series of bulk components, non-polar and polar OMMs grouped by vapor pressure at 298.15 K ($p^{o,*}_L$, atm) or source, and the light absorption of WSOC and MEOC in $PM_{2.5}$ and PM_{10}. Appendix A Figs. S7–S10 present comparisons between collocated measurements of the abovementioned species and light absorption in PM of the same size ($PM_{2.5}$ or PM_{10}) for validation.

In Appendix A Table S5, the seasonal variations of speciated compounds and aerosol extract absorption for $PM_{2.5}$ are generally consistent with our previous observations (Yang et al., 2021; Gou et al., 2021; Qin et al., 2021; Xie et al., 2022c; Feng et al., 2023b). The reconstructed $PM_{2.5}$ and PM_{10} doubled in winter due in large part to the increase in NO_3^-. The mass contributions of NO_3^- to reconstructed $PM_{2.5}$ and PM_{10} in summer decreased from > 25% to 11.2% ± 7.33% and 16.1% ± 6.43%, respectively, after July 30, 2020 (T > 29°C, Appendix A Fig. S1), and were negatively related to ambient temperature (Appendix A Fig. S11). WSOC accounted for ~ 70% and ~ 55% of OC in $PM_{2.5}$ and PM_{10} on average, and the WSOC/OC ratio showed no significant difference between summer and winter ($p > 0.05$). Receptor-based source apportionment showed that biomass burning and secondary formation are the two main sources of WSOC in $PM_{2.5}$ during wintertime at the same location (Feng et al., 2023b). Considering the sharp increase in biomass burning tracers from summer to winter (Appendix A Table S5), the elevated emissions from biomass burning and the associated aging processes are responsible for the higher WSOC concentration in winter than in summer. The contributions of WSON to WSTN were higher in summer ($PM_{2.5}$, 11.7% ± 7.06%; PM_{10}, 24.5% ± 7.02%) than in winter (PM_{10}, 17.9% ± 5.58%), and the concentrations of WSON and NH_4^+-N + NO_3^--N were strongly correlated in summer ($r = 0.76$ and 0.91, $p < 0.01$). Based on the PMF analysis of WSON and the linkages between WSON and estimated aerosol liquid water, Xu et al. (2020) concluded that the reactions of NH_4^+ and reactive nitrogen with biogenic volatile organic compounds (VOCs) in the aqueous phase are a key formation pathway for WSON in submicron PM. Laboratory studies also provided evidence for the formation of oxidized (e.g., organic nitrates, nitrophenols) and reduced organic nitrogen through gaseous and aqueous reactions (Fry et al., 2014; Lin et al., 2015b; Stangl and Johnston, 2017). Therefore, NH_4^+ and NO_3^- or their precursors (NH_3 and NO_2) were likely involved in the formation of WSON in summer Nanjing.

The mass fractions of low-volatility ($p^{o,*}_L < 10^{-10}$ atm) n-alkanes and PAHs in $PM_{2.5}$ and PM_{10} were significantly ($p < 0.05$) greater in summer ($PM_{2.5}$, 60.1% ± 10.4% and 68.8% ± 10.7%; PM_{10}, 74.2% ± 6.29% and 72.4% ± 7.98%) than in winter ($PM_{2.5}$, 51.3% ± 7.56% and 65.8% ± 8.18%; PM_{10}, 51.5% ± 6.76% and 63.4% ± 7.76%), which could be attributed to the evaporation of more volatile n-alkanes and PAHs in summer. Hopanes and steranes occurred mainly in the particle phase

(Gou et al., 2021) and exhibited the least seasonal variability among non-polar OMMs. Concentrations of isoprene SOA products were more than ten times higher in summer than in winter (Appendix A Tables S5 and S7), as isoprene is emitted mainly from deciduous trees and has maximum concentrations in summer (Wang et al., 2020). Biomass fuels (e.g., straw and wood) were widely used for cooking and heating in rural China in winter (Chen et al., 2017), resulting in a pattern of high winter and low summer levels of biomass burning tracers (Appendix A Tables S5 and S7). Unlike the seasonality of $PM_{2.5}$-bound sugar polyols and saccharides that was partially influenced by biomass burning (Medeiros et al., 2006; Marynowski and Simoneit, 2022), PM_{10}-bound sugars are more than twice as high in summer as in winter. This is because soil microorganisms and vegetation products are important sources of sugars in coarse PM and are increasingly emitted during the growing season (Simoneit et al., 2004; Bauer et al., 2008; Burshtein et al., 2011; Verma et al., 2018). In Norway, sugars were also primarily associated with coarse PM with maximum concentrations in summer, while a shift towards fine PM was observed in winter due to wood burning (Yttri et al., 2007). Owning to the increased emissions from biofuel combustion and anthropogenic SOA in winter (Li et al., 2015; Ding et al., 2017), which contained strong BrC chromophores, the rates of increase for $Abs_{365,w}$ and $Abs_{365,m}$ from summer to winter were larger than those for WSOC and OC, respectively, leading to elevated $MAE_{365,w}$ and $MAE_{365,m}$ values in winter (Appendix A Table S5).

2.2. *Comparisons between $PM_{2.5}$ and PM_{10}*

Appendix A Figs. S7–S10 show that most measured species and aerosol extract absorption have good collocated precision with no significant difference ($p > 0.05$) in mean values. Only the scatter data for *n*-alkanes and PAHs with $p^{o,*}_L > 10^{-8}$ atm, as well as steranes and hopanes, deviated from the identity line due to their low concentrations (Appendix A Fig. S8a, e, and l). Given the uncertainties in sampling and laboratory analysis, the differences in measured species and aerosol extract absorption between $PM_{2.5}$ and PM_{10}, representing the contribution of coarse particles, are evaluated using linear regressions in Figs. 1–3 and Appendix A Fig. S12.

2.2.1. *Bulk components*

The average concentrations of NH_4^+ and WSOC exhibited no significant difference ($p > 0.05$) between $PM_{2.5}$ and PM_{10} in both summer and winter. In Fig. 1**a**, almost all the scatter data of NH_4^+ fall along the identity line, indicating that PM_{10}-bound NH_4^+ is mainly enriched in $PM_{2.5}$ in northern Nanjing. Fig. 1**g** shows that coarse PM in some PM_{10} samples makes a significant contribution to WSOC in winter. The increase in WSOC and biomass burning tracers in coarse PM occurred at the same time (January 13–25, 2021). In addition, the average $PM_{10}/PM_{2.5}$ ratios of WSOC and biomass burning tracers during this period were 1.48 ± 0.17 and 1.55 ± 0.23, respectively, with no significant difference ($p > 0.05$). As shown in Fig. 3**b** and Appendix A Fig. S5f, substantial biomass burning tracers were associated with coarse PM when their concentrations in PM_{10} peaked in winter. Since emissions from biomass burning and dust particles can mix well during the transport (Hand et al., 2010; Zhou et al., 2018), the increased coarse fraction of WSOC in winter was attributed to excessive biomass burning activities.

The concentrations of NO_3^-, SO_4^{2-}, OC, and WSTN in $PM_{2.5}$ and PM_{10} showed strong correlations ($r > 0.70$, $p < 0.01$), and their regression slopes are not far from unity (Fig. 1**b, c, e,** and **h**), as these species were majorly distributed in fine PM (Appendix A Table S5). The presence of NO_3^- and SO_4^{2-} in coarse PM is caused by the conversion of NO_X and SO_2 on PM surfaces toward HNO_3 and H_2SO_4, followed by neutralization with PM-bound alkali salts (e.g., $CaCO_3$) but not NH_3 gas (Wu et al., 2020b). According to the average concentrations of NO_3^- and SO_4^{2-} in $PM_{2.5}$ and PM_{10}, coarse PM contributed 39.2% to NO_3^- in summer, about twice as much as in winter (21.6%). This is because NO_3^- primarily exists as semi-volatile NH_4NO_3 in $PM_{2.5}$ and non-volatile forms [e.g., $Ca(NO_3)_2$] in coarse PM. In contrast, the mass fraction of SO_4^{2-} in coarse PM was higher in winter (29.3%) than in summer (16.5%), which can be attributed to the enhanced formation of SO_4^{2-} by heterogeneous reaction of SO_2 on dust surfaces in winter (Liu et al., 2017; Wang et al., 2022). OC fractions associated with coarse PM were comparable in summer (19.0%) and winter (19.5%), but the scatter data of OC showed a stronger correlation in winter ($r = 0.90$, Fig. 1**e**), suggesting that OC sources in fine and coarse PM differ more in summer. The average EC concentration in PM_{10} was similar to that in $PM_{2.5}$ in winter but more than 40% higher in summer (Appendix A Table S5), and the weak correlation between $PM_{2.5}$ and PM_{10} in summer ($r = 0.33$, Fig. 1**f**) suggests different origins. We suspected that resuspended road dust containing EC from combustion emissions could be an important indirect source of EC in summer.

Ca^{2+} is commonly used to indicate sources of crustal soil or dust resuspension (Brahney et al., 2013), and its concentrations were predominantly distributed in coarse PM in both summer (87.7%) and winter (73.9%). WSTN consisted mainly of NH_4^+-N and NO_3^--N, and the difference between $PM_{2.5}$ and PM_{10} was determined by NO_3^- content. Although WSON mostly resided in coarse PM, its concentrations in $PM_{2.5}$ and PM_{10} were strongly correlated in summer ($r = 0.73$; Fig. 1**i**). Among all the bulk components, NH_4^+ has the highest correlation ($r = 0.73$–0.93) with WSON, followed by NO_3^- ($r = 0.56$–0.91) and SO_4^{2-} ($r = 0.45$–0.71, $p < 0.01$). However, no strong correlation was observed between WSON and Ca^{2+} ($r < 0.30$) or secondary OC (EC tracer method, $r < 0.30$). As mentioned in Section 2.1, secondary ions or their precursors could be involved in the formation of WSON, but its accumulation in coarse particles is not clear. Previous studies have found that the size distribution pattern of WSON was location- and time-dependent and dominated in either fine or coarse mode, and the transport of processed dust could be an important source of WSON (Chen et al., 2010; Violaki and Mihalopoulos, 2010; Miyazaki et al., 2014; Tsagkaraki et al., 2021). To adequately determine the size distribution and sources of WSON, further studies are needed to identify and quantify the source-specific WSON compounds.

2.2.2. *Organic molecular markers*

The average concentrations of volatile *n*-alkanes, PAHs, and oxy-PAHs ($p^{o,*}_L > 10^{-8}$ atm) were similar between $PM_{2.5}$ and PM_{10} in summer with no significant difference ($p > 0.05$; Ap-

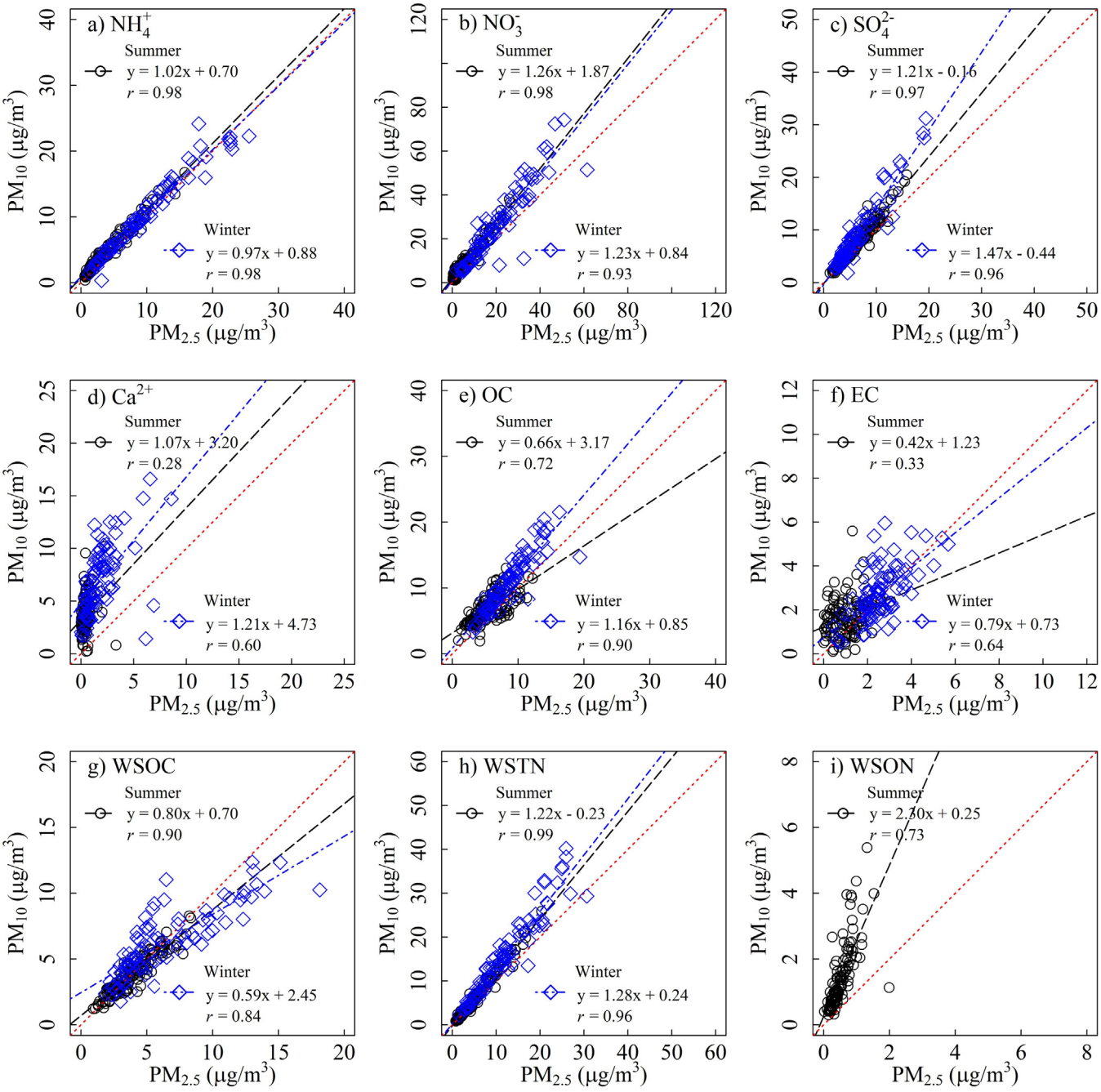

Fig. 1 – Comparisons of measured bulk components of $PM_{2.5}$ and PM_{10} collected synchronously in summer and winter.

pendix A Table S5). However, caution should be taken when comparing the time series of volatile *n*-alkanes and PAHs in $PM_{2.5}$ with those in PM_{10} because of their low concentrations (Fig. 2**a, e** and Appendix A Fig. S8a, e). Except for the *n*-alkanes with $p^{o,*}_L < 10^{-10}$ atm, whose average concentration in $PM_{2.5}$ explained only about half of that in PM_{10} in summer, the concentration time series of the less volatile *n*-alkanes, PAHs, and oxy-PAHs with $p^{o,*}_L < 10^{-8}$ atm showed good agreement between $PM_{2.5}$ and PM_{10} throughout the period (Fig. 2 and Appendix A Figs. S2–S4). These results suggest that non-combustion sources, including tire-wear debris, plant leaf wax, etc. (Rogge et al., 1993a, 1993b), contributed significantly to PM_{10}-bound low-volatility *n*-alkanes ($p^{o,*}_L < 10^{-10}$ atm) in summer, whereas anthropogenic activities (e.g., fossil fuel and biomass combustion) dominated emissions of *n*-alkanes, PAHs, and oxy-PAHs in other circumstances. Steranes and hopanes are commonly used to identify combustion of lubricating oil in motor vehicles (Shrivastava et al., 2007; Kleeman et al., 2008), and the stronger correlation of their total concentrations between $PM_{2.5}$ and PM_{10} in winter ($r = 0.72$) indicates the dominance of combustion sources (Fig. 2**l**). Furthermore, the mass fraction of steranes and hopanes in coarse PM increased substantially from summer (14.0%) to winter (42.6%), indicating the mixing of combustion emissions and

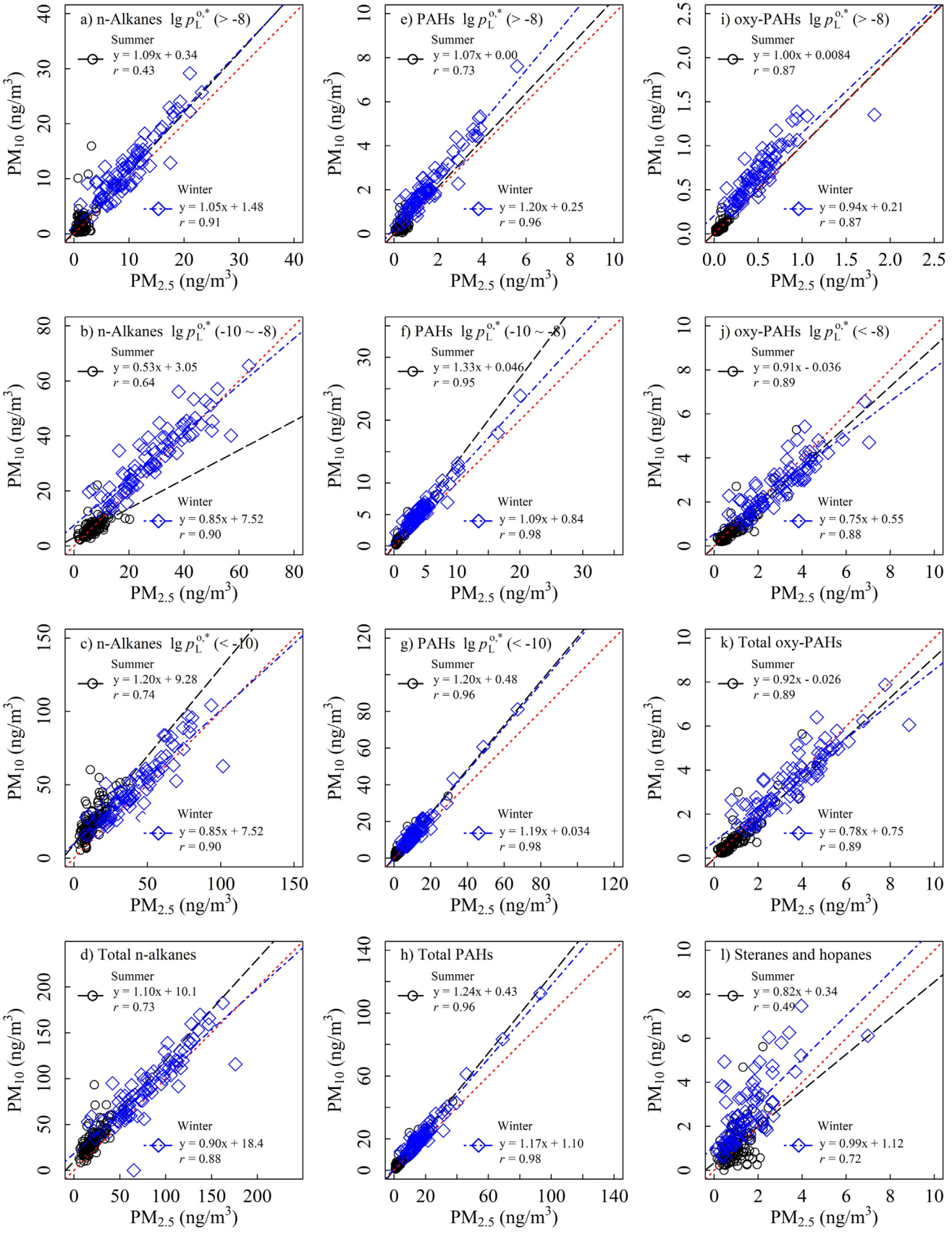

Fig. 2 – Comparisons of non-polar OMMs, grouped by vapor pressure, between $PM_{2.5}$ and PM_{10} collected synchronously in summer and winter.

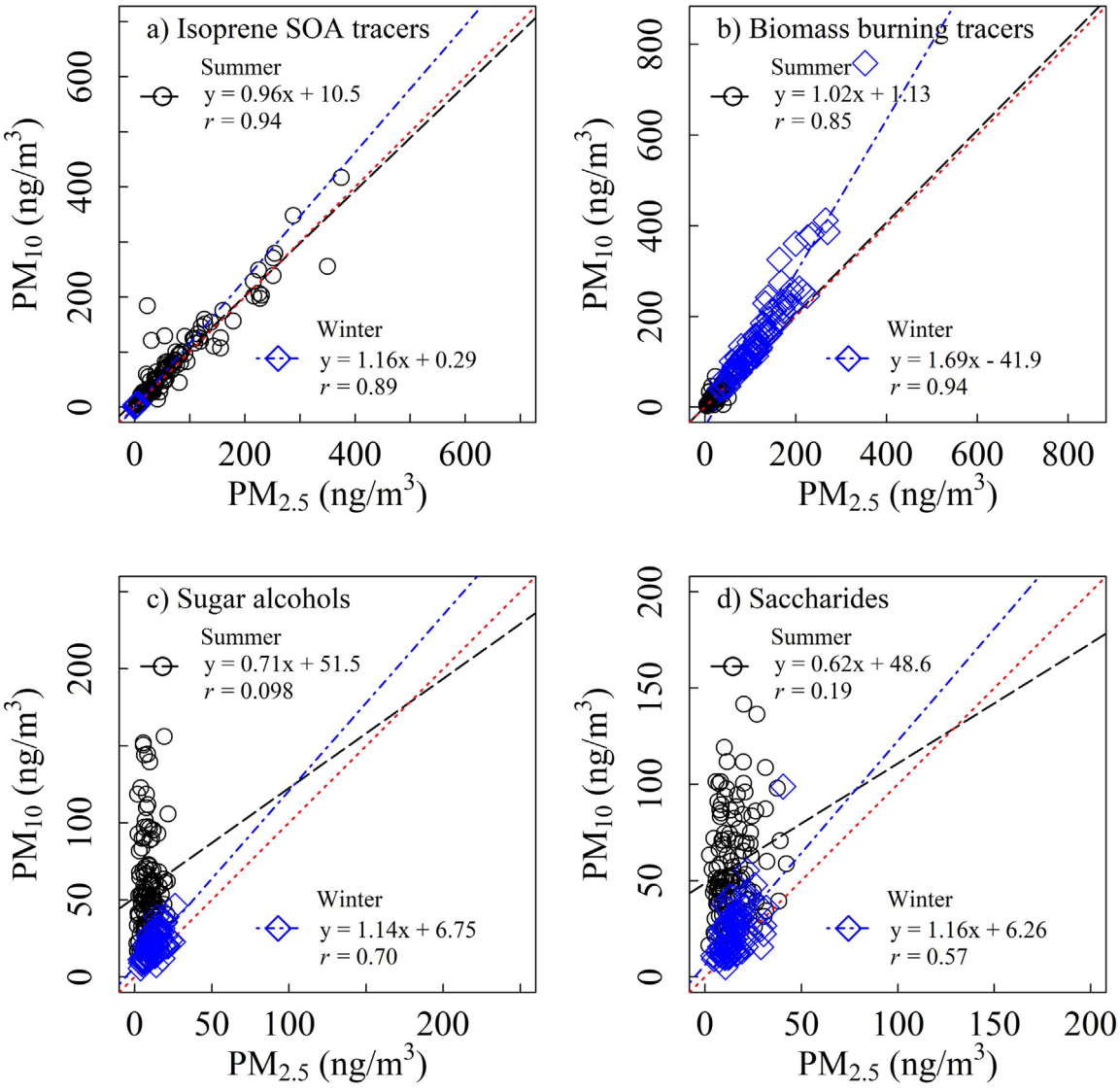

Fig. 3 – Comparisons of polar OMMs, grouped by sources, between $PM_{2.5}$ and PM_{10} collected synchronously in summer and winter.

crustal dust during wintertime (Xie et al., 2022a; Feng 2023a). Wang et al. (2009, 2012) also observed a bimodal size distribution of hopanes and low-volatility *n*-alkanes (e.g., *n*-C31) for mountain aerosols in summer, while fossil fuel-derived *n*-alkanes and PAHs were mainly loaded in the fine mode.

In Appendix A Fig. S5, isoprene SOA and biomass burning tracers in $PM_{2.5}$ have similar concentration time series as in PM_{10}, and the regressions in summer almost overlap with the identity line (Fig. 3). These two groups of polar OMMs existed mainly in $PM_{2.5}$ but had opposite seasonality. Huang et al. (2020) raised that the oxygenated organic aerosols in coarse PM were formed by heterogeneous reactions of biogenic VOCs rather than by primary biological materials on soil dust. However, the formation of the measured isoprene SOA products requires acidic aerosols to catalyze the uptake of gaseous intermediates (Surratt et al., 2010; Lin et al., 2013; Lei et al., 2022), and $PM_{2.5}$ is composed mainly of ammonium salts [e.g., NH_4NO_3 and $(NH_4)_2SO_4$] and is more acidic than coarse PM (Pan et al., 2018). As mentioned in *Section* 2.2.1, the concentrations of biomass burning tracers in PM_{10} became significantly higher than those in $PM_{2.5}$ once there were intensive biomass burning activities, leading to an increase in the coarse fraction (26.4%) in winter compared to that in summer (7.69%). Sugar alcohols and saccharides were mainly distributed in coarse PM during summer (> 70%), and the weak correlations between $PM_{2.5}$ and PM_{10} indicated that these species had different sources in fine and coarse PM during the growing season. The concentration time series of sugar alcohols and saccharides in $PM_{2.5}$ and PM_{10} became similar in winter with moderate correlations ($r > 0.50$, Fig. 3**c, d** and Appendix A Fig. S5), and significant correlations ($r > 0.50, p < 0.01$) were also observed between these two groups of sugar polyols and biomass burning tracers for PM_{10}, particularly after January 13, 2021 with excessive biomass burning. As shown in Appendix A Fig. S13, the fire spots are highly concentrated on the backward trajectories of selected winter samples with

high levoglucosan concentrations (226–369 ng/m^3). These results support that biomass burning is a potentially important source of sugar polyols in winter.

2.2.3. *WSOC and MEOC absorption*

Interestingly, PM_{10} had significantly higher ($p < 0.01$) average $Abs_{365,w}$ values (summer, 1.71 ± 0.82 Mm^{-1}; winter, 6.04 ± 2.51 Mm^{-1}) than $PM_{2.5}$ (summer, 1.41 ± 0.66 Mm^{-1}; winter, 4.73 ± 1.97 Mm^{-1}), whereas WSOC in $PM_{2.5}$ and PM_{10} exhibited less difference in average concentrations and temporal variations (Appendix A Table S5 and Fig. 1g). There is evidence that the light absorption of aerosol extracts in water increases with solution pH, as the deprotonation of BrC chromophores at higher pH leads to increased aromaticity and conjugation (Phillips et al., 2017; Qin et al., 2022), and the pH of aerosol extracts tends to be higher under the influence of dust (Wang et al., 2011; Shi et al., 2017). The $Abs_{365,m}$ values of $PM_{2.5}$ and PM_{10} had comparable average values and similar time series (Appendix A Table S5 and Appendix A Fig. S6b, f), and the regressions shown in Appendix A Fig. S12b indicate that methanol-extractable BrC chromophores are predominantly present in fine PM, consistent with observations in Atlanta (Liu et al., 2013) and Xi'an (Wu et al., 2020a). Considering that the uncertainty of $Abs_{365,m}$ derived from collocated measurements was up to 20% (Xie et al., 2022c), the lower average $Abs_{365,m}$ value of PM_{10} compared to $PM_{2.5}$ in summer with an average relative percent difference of 21.5% ± 19.4% was possibly due to the uncertainties in sampling and light absorbance analysis. Because the organic materials in coarse PM that could be dissolved by methanol had ignorable light absorption, the $MAE_{365,m}$ values of $PM_{2.5}$ (summer, 0.74 ± 0.33 m^2/g C; winter, 1.23 ± 0.26 m^2/g C) were significantly higher ($p < 0.01$) than those of PM_{10} (summer, 0.49 ± 0.15 m^2/g C; winter, 0.99 ± 0.25 m^2/g C; Appendix A Table S5).

2.3. *Source apportionment*

2.3.1. *Overview of PMF results*

Finally, for both the $PMF_{2.5}$ and PMF_{10} data sets, an 8-factor solution was chosen because it contained the most physically meaningful factors and was robust to rotational ambiguity and random error (Appendix A Text S3). Appendix A Table S8 shows good agreement between the input data and PMF estimates of aerosol extract absorption and bulk species. Seven of the eight factors from $PMF_{2.5}$ and PMF_{10} solutions are paired by normalized profiles in Appendix A Fig. S14 and are identified as biomass burning, lubricating oil combustion, coal combustion, biogenic emission, isoprene oxidation, secondary inorganics, and dust resuspension. A tire-wear debris factor constituted by heavy *n*-alkanes was resolved in the $PMF_{2.5}$ solution, and a secondary sulfate factor was separated in the PMF_{10} solution only. Compared with our previous study, in which nine factors for the absorption of aerosol extracts and bulk components in $PM_{2.5}$ were determined using one-year measurement data of total OMMs (gas + particle phases; Xie et al., 2022c), the low MW *n*-alkane and PAH factor was not identified here, as OMMs with $p^{o,*}_L > 10^{-8}$ atm were excluded to avoid influences of gas-to-particle partitioning. In this work, the $PMF_{2.5}$ solution combined secondary nitrate and sulfate into a secondary inorganics factor, while the remaining factors exhibited similar source profiles as in the previous study. The average absolute and relative contributions of each factor to light absorption and bulk components are provided in Appendix A Tables S9 and S10. Fig. 4 illustrates the distributions of factor contributions to WSOC, OC, $Abs_{365,w}$, and $Abs_{365,m}$.

2.3.2. *Factor interpretation and comparisons*

In Appendix A Fig. S14, the biomass burning factor in the two solutions is identified by the highest loadings of levoglucosan ($PMF_{2.5}$ 48.9%, PMF_{10} 67.5%). It also contained the highest proportions of light *n*-alkanes (*n*-C22–*n*-C27, 31.8%–77.6%) and PAHs (fluoranthene and pyrene, 46.0%–51.8%). Consistent with the seasonality of biomass burning activities for heating purposes, this factor contributed most to $Abs_{365,w}$ and $Abs_{365,m}$ in winter (Fig. 4), but made trivial contributions to light absorption and bulk components in summer (Appendix A Tables S9 and S10). The two factors, characterized by the strong presence of steranes/hopanes and PAHs, indicated a relationship with the combustion of lubricating oil and coal, respectively, and they were not major contributors of aerosol extract absorption. The biogenic emission factor of the PMF_{10} solution exhibited higher loadings of sugar polyols than that of the $PMF_{2.5}$ solution (Appendix A Fig. S14d), because sugar polyols existed mainly in coarse PM and were primarily derived from biogenic sources. Its contributions to WSOC and OC showed a pattern of high summer and low winter values for both the $PMF_{2.5}$ and PMF_{10} solutions (Fig. 4), although the seasonality of sugar polyol concentrations was different between $PM_{2.5}$ and PM_{10}. The isoprene oxidation factor was characterized by the highest loadings of the three isoprene SOA products. Owning to the large difference in concentrations between summer and winter (Appendix A Table S5), the isoprene oxidation factor had discernable contributions to WSOC, OC, and their light absorption only in summer (Fig. 4). It has been demonstrated that light-absorbing oligomers formed by reactive uptake and multiphase chemistry of isoprene epoxy diols under dry and acidic conditions could be a potential BrC source (Lin et al., 2014; Nakayama et al., 2015). Since only isoprene SOA tracers were included and PMF fitted the input data, the contributions of other biogenic and anthropogenic SOA to organic aerosols and their light absorption could be apportioned to isoprene oxidation, secondary inorganics, and secondary sulfate factors. Given that the reactions of SOA and nitrogen-containing species (e.g., NH_3, NH_4^+) in the aqueous phase are an important formation pathway for BrC chromophores (Updyke et al., 2012; Powelson et al., 2014; Lin et al., 2015a) and the ambient PM in northern Nanjing has high water content (18.8 ± 19.4 μg/m^3; Yang et al., 2021), the secondary inorganics factor with considerable contributions to $Abs_{365,w}$ and $Abs_{365,m}$ (Fig. 4) may also indicate the process of BrC formation through aqueous phase reactions.

Unlike the $PMF_{2.5}$ solution, the dust resuspension factor of the PMF_{10} solution contained more than 30% OC, EC, and WSOC in addition to Ca^{2+} (Appendix A Fig. S14g). This factor was also characterized by the *n*-alkane pattern with odd-to-even carbon number predominance from *n*-C_{27} to *n*-C_{35}, resembling *n*-alkane profiles of leaf abrasion products and paved road dust (Rogge et al., 1993a, 1993b). Comparison of the dust resuspension factor between $PMF_{2.5}$ and PMF_{10} ex-

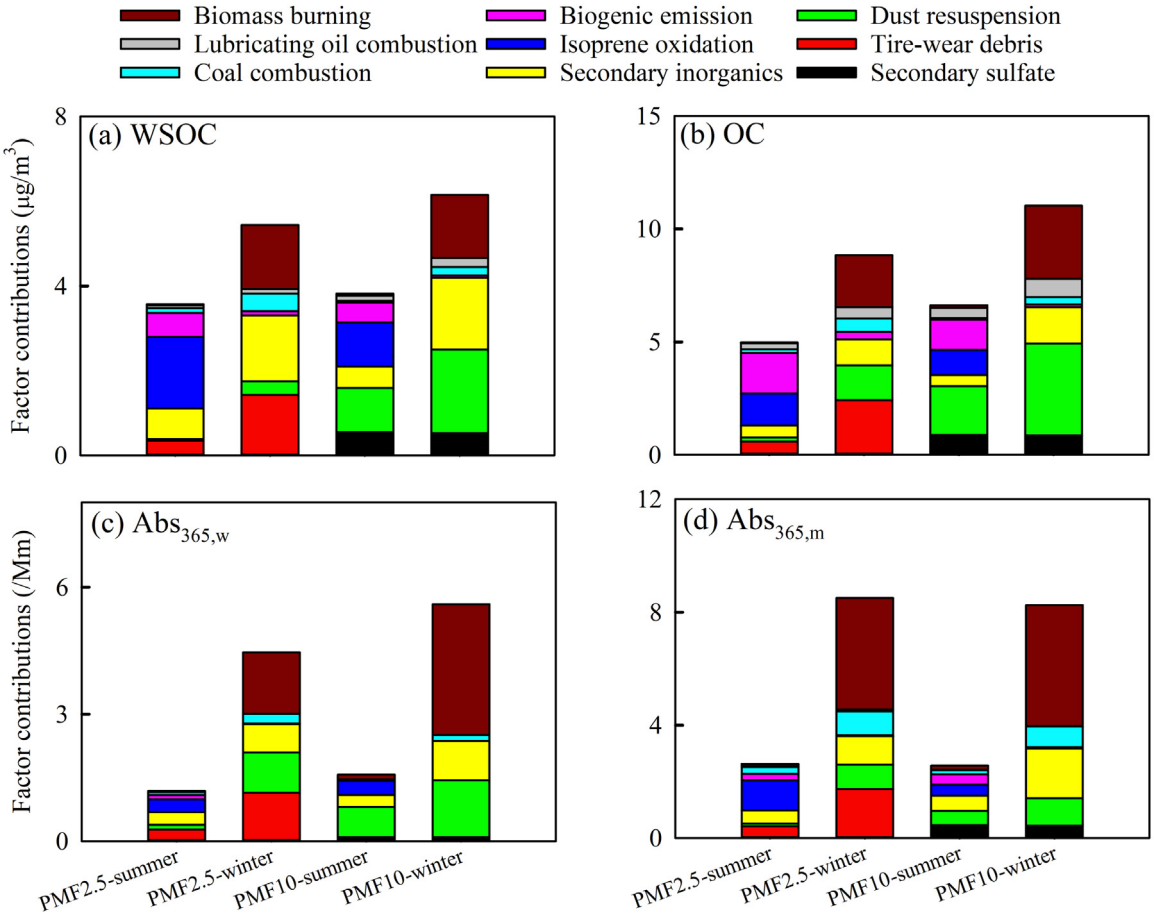

Fig. 4 – Factor contribution distributions of (a) water-soluble organic carbon (WSOC), (b) OC, (c) $Abs_{365,w}$, and (d) $Abs_{365,m}$ derived from $PMF_{2.5}$ and PMF_{10} solutions.

plained a large part of the difference in OC and EC concentrations between $PM_{2.5}$ and PM_{10}. Besides heavy *n*-alkanes, the tire-wear debris factor of the $PMF_{2.5}$ solution was also loaded with 25% levoglucosan. Thus, the $Abs_{365,w}$ and $Abs_{365,m}$ assigned to this factor (Fig. 4) were jointly contributed by road dust and biomass burning, indicating a source of transported road dust polluted by biomass burning plumes (Zhou et al., 2018; Ghosh et al., 2019). The secondary sulfate factor of PMF_{10} solution contained mainly SO_4^{2-} and about 20% NH_4^+, Ca^{2+}, and EC. Since SO_4^{2-} was partially distributed in the coarse PM (Fig. 1**c**), the factor profile supported the presence of heterogenous transformation of SO_2 on dust surfaces.

3. Conclusions

In this work, synchronous sampling of $PM_{2.5}$ and PM_{10} was conducted in the summer of 2020 and winter of 2020/2021 in northern Nanjing, China. Each pair of samples was analyzed for bulk components, OMMs, and solvent extract absorption. Comparisons between $PM_{2.5}$ and PM_{10} showed that NH_4^+ and WSOC were almost entirely distributed in fine PM. However, more WSOC shifted to coarse PM when excessive biomass burning occurred. NO_3^-, SO_4^{2-}, OC, and WSTN were mainly in fine PM, and the presence of NO_3^-, SO_4^{2-}, and WSTN in coarse PM was ascribed to the conversion of precursors NO_X and SO_2 at dust surfaces. Owning to the influence of non-combustions sources, coarse PM contributed about 50% of the low-volatility *n*-alkanes in summer. Other non-polar OMMs exhibited strong correlations between $PM_{2.5}$ and PM_{10} in winter, indicating the dominance of anthropogenic sources. The seasonality and size distribution of polar OMMs coincided with their source types and emission intensity. The coarse fraction of biomass burning tracers in winter increased at their maximum concentrations, and biomass burning became an important source of sugar polyols in winter. PM_{10} extracts in water showed stronger light absorption than $PM_{2.5}$ extracts due to the influence of alkaline substances in coarse PM on pH. Since MEOC in coarse PM had ignorable light absorption, the mass absorption efficiency of MEOC was significantly higher in $PM_{2.5}$ than in PM_{10}.

Source apportionment results showed that biomass burning contributed the largest fraction of BrC absorption in winter. Primary biogenic emissions and biogenic SOA had discernable contributions to organic aerosols only in summer. In the absence of source-specific OMMs, the fractions of WSOC, OC, and their light absorption attributable to the secondary inorganics factor could be related to the aqueous-phase mechanism for anthropogenic SOA formation. The dust resuspension factor of PMF_{10} solution contributed more OC and EC than

that of $PMF_{2.5}$ solution, which partly explained the difference in OC and EC concentrations between $PM_{2.5}$ and PM_{10}. Due to the difference in concentration time series of input species between $PM_{2.5}$ and PM_{10}, the tire-wear abrasion factor, representing joint influences of road dust and biomass burning, was identified only in the $PMF_{2.5}$ solution. The PMF_{10} solution resolved a secondary sulfate factor indicating heterogeneous processes on coarse PM surfaces. Considering the role that coarse PM plays in the mass contribution to PM_{10} and in the production of secondary aerosols, more efforts should be exerted to control dust emissions.

Declaration of Competing Interest

The authors declare that they have no known competing financial interests or personal relationships that could have appeared to influence the work reported in this paper.

Acknowledgments

This work was supported by the National Natural Science Foundation of China (Nos. 42007325 and 42177211). The authors gratefully acknowledge the NOAA Air Resources Laboratory (ARL) for the provision of the HYSPLIT transport and dispersion model and/or READY website (https://www.ready.noaa.gov) used in this publication, and the use of data and/or imagery from NASA's Fire Information for Resource Management System (FIRMS) (https://earthdata.nasa.gov/firms), part of NASA's Earth Observing System Data and Information System (EOSDIS).

Appendix A Supplementary data

Supplementary material associated with this article can be found in the online version at doi:10.1016/j.jes.2024.04.038.

References

Bauer, H., Claeys, M., Vermeylen, R., Schueller, E., Weinke, G., Berger, A., et al., 2008. Arabitol and mannitol as tracers for the quantification of airborne fungal spores. Atmos. Environ. 42 (3), 588–593.

Brahney, J., Ballantyne, A.P., Sievers, C., Neff, J.C., 2013. Increasing Ca^{2+} deposition in the western US: the role of mineral aerosols. Aeolian Res. 10, 77–87.

Burshtein, N., Lang-Yona, N., Rudich, Y., 2011. Ergosterol, arabitol and mannitol as tracers for biogenic aerosols in the eastern Mediterranean. Atmos. Chem. Phys. 11 (2), 829–839.

Cao, J., Xu, H., Xu, Q., Chen, B., Kan, H., 2012. Fine particulate matter constituents and cardiopulmonary mortality in a heavily polluted Chinese city. Environ. Health Perspect. 120 (3), 373–378.

Chen, H.-Y., Chen, L.-D., Chiang, Z.-Y., Hung, C.-C., Lin, F.-J., Chou, W.-C., et al., 2010. Size fractionation and molecular composition of water-soluble inorganic and organic nitrogen in aerosols of a coastal environment. J. Geophys. Res. Atmos. 115, D22307.

Chen, J., Li, C., Ristovski, Z., Milic, A., Gu, Y., Islam, M.S., et al., 2017. A review of biomass burning: emissions and impacts on air quality, health and climate in China. Sci. Total Environ. 579, 1000–1034.

Ding, X., Zhang, Y.Q., He, Q.F., Yu, Q.Q., Wang, J.Q., Shen, R.Q., et al., 2017. Significant increase of aromatics-derived secondary organic aerosol during fall to winter in China. Environ. Sci. Technol. 51 (13), 7432–7441.

Feng, W., Shao, Z., Wang, Q.g., Xie, M., 2023a. Size-resolved light-absorbing organic carbon and organic molecular markers in Nanjing, east China: seasonal variations and sources. Environ. Pollut. 332, 122006.

Feng, W., Wang, X., Shao, Z., Liao, H., Wang, Y., Xie, M., 2023b. Time-resolved measurements of $PM_{2.5}$ chemical composition and brown carbon absorption in Nanjing, east China: diurnal variations and organic tracer-based PMF analysis. J. Geophys. Res. Atmos. 128 (18) e2023JD039092.

Fry, J.L., Draper, D.C., Barsanti, K.C., Smith, J.N., Ortega, J., Winkler, P.M., et al., 2014. Secondary organic aerosol formation and organic nitrate yield from NO_3 oxidation of biogenic hydrocarbons. Environ. Sci. Technol. 48 (20), 11944–11953.

Ghosh, A., Roy, A., Chatterjee, A., Das, S.K., Ghosh, S.K., Raha, S., 2019. Impact of biomass burning plumes on the size-segregated aerosol chemistry over an urban atmosphere at Indo-Gangetic plain. Aerosol Air Qual. Res. 19 (1), 163–180.

Gou, Y., Qin, C., Liao, H., Xie, M., 2021. Measurements, gas/particle partitioning, and sources of nonpolar organic molecular markers at a suburban site in the west Yangtze River Delta. China. J. Geophys. Res. Atmos. 126 (19) e2020JD034080.

Hand, V.L., Capes, G., Vaughan, D.J., Formenti, P., Haywood, J.M., Coe, H., 2010. Evidence of internal mixing of African dust and biomass burning particles by individual particle analysis using electron beam techniques. J. Geophys. Res. Atmos. 115, D13301.

Hong, C., Zhang, Q., Zhang, Y., Davis, S.J., Zhang, X., Tong, D., et al., 2020. Weakening aerosol direct radiative effects mitigate climate penalty on Chinese air quality. Nat. Clim. Change 10 (9), 845–850.

Huang, X., Liu, Z., Liu, J., Hu, B., Wen, T., Tang, G., et al., 2017. Chemical characterization and source identification of $PM_{2.5}$ at multiple sites in the Beijing–Tianjin–Hebei region, China. Atmos. Chem. Phys. 17 (21), 12941–12962.

Huang, X.-F., Dai, J., Zhu, Q., Yu, K., Du, K., 2020. Abundant biogenic oxygenated organic aerosol in atmospheric coarse particles: plausible sources and atmospheric implications. Environ. Sci. Technol. 54 (3), 1425–1430.

Kleeman, M.J., Riddle, S.G., Robert, M.A., Jakober, C.A., 2008. Lubricating oil and fuel contributions to particulate matter emissions from light-duty gasoline and heavy-duty diesel vehicles. Environ. Sci. Technol. 42 (1), 235–242.

Lei, Z., Chen, Y., Zhang, Y., Cooke, M.E., Ledsky, I.R., Armstrong, N.C., et al., 2022. Initial pH governs secondary organic aerosol phase state and morphology after uptake of isoprene epoxydiols (IEPOX). Environ. Sci. Technol. 56 (15), 10596–10607.

Li, B., Zhang, J., Zhao, Y., Yuan, S., Zhao, Q., Shen, G., et al., 2015. Seasonal variation of urban carbonaceous aerosols in a typical city Nanjing in Yangtze River Delta. China. Atmos. Environ. 106, 223–231.

Lin, P., Laskin, J., Nizkorodov, S.A., Laskin, A., 2015a. Revealing brown carbon chromophores produced in reactions of methylglyoxal with ammonium sulfate. Environ. Sci. Technol. 49 (24), 14257–14266.

Lin, P., Liu, J., Shilling, J.E., Kathmann, S.M., Laskin, J., Laskin, A., 2015b. Molecular characterization of brown carbon (BrC) chromophores in secondary organic aerosol generated from photo-oxidation of toluene. Phys. Chem. Chem. Phys. 17 (36), 23312–23325.

Lin, Y.-H., Budisulistiorini, S.H., Chu, K., Siejack, R.A., Zhang, H., Riva, M., et al., 2014. Light-absorbing oligomer formation in secondary organic aerosol from reactive uptake of isoprene epoxydiols. Environ. Sci. Technol. 48 (20), 12012–12021.
Lin, Y.-H., Zhang, H., Pye, H.O.T., Zhang, Z., Marth, W.J., Park, S., et al., 2013. Epoxide as a precursor to secondary organic aerosol formation from isoprene photooxidation in the presence of nitrogen oxides. Proc. Natl. Acad. Sci. 110 (17), 6718–6723.
Liu, J., Bergin, M., Guo, H., King, L., Kotra, N., Edgerton, E., et al., 2013. Size-resolved measurements of brown carbon in water and methanol extracts and estimates of their contribution to ambient fine-particle light absorption. Atmos. Chem. Phys. 13 (24), 12389–12404.
Liu, J., Zheng, Y., Geng, G., Hong, C., Li, M., Li, X., et al., 2020. Decadal changes in anthropogenic source contribution of $PM_{2.5}$ pollution and related health impacts in China, 1990–2015. Atmos. Chem. Phys. 20 (13), 7783–7799.
Liu, Z., Xie, Y., Hu, B., Wen, T., Xin, J., Li, X., et al., 2017. Size-resolved aerosol water-soluble ions during the summer and winter seasons in Beijing: formation mechanisms of secondary inorganic aerosols. Chemosphere 183, 119–131.
Marynowski, L., Simoneit, B.R.T., 2022. Saccharides in atmospheric particulate and sedimentary organic matter: status overview and future perspectives. Chemosphere 288, 132376.
Medeiros, P.M., Conte, M.H., Weber, J.C., Simoneit, B.R.T., 2006. Sugars as source indicators of biogenic organic carbon in aerosols collected above the Howland Experimental Forest, Maine. Atmos. Environ. 40 (9), 1694–1705.
Miyazaki, Y., Fu, P., Ono, K., Tachibana, E., Kawamura, K., 2014. Seasonal cycles of water-soluble organic nitrogen aerosols in a deciduous broadleaf forest in northern Japan. J. Geophys. Res. Atmos. 119 (3), 1440–1454.
Nakayama, T., Sato, K., Tsuge, M., Imamura, T., Matsumi, Y., 2015. Complex refractive index of secondary organic aerosol generated from isoprene/NOx photooxidation in the presence and absence of SO_2. J. Geophys. Res. Atmos. 120 (15), 7777–7787.
Pan, X., Uno, I., Wang, Z., Yamamoto, S., Hara, Y., Wang, Z., 2018. Seasonal variabilities in chemical compounds and acidity of aerosol particles at urban site in the west Pacific. Environ. Pollut. 237, 868–877.
Phillips, S.M., Bellcross, A.D., Smith, G.D., 2017. Light absorption by brown carbon in the Southeastern United States is pH-dependent. Environ. Sci. Technol. 51 (12), 6782–6790.
Powelson, M.H., Espelien, B.M., Hawkins, L.N., Galloway, M.M., De Haan, D.O., 2014. Brown carbon formation by aqueous-phase carbonyl compound reactions with amines and ammonium sulfate. Environ. Sci. Technol. 48 (2), 985–993.
Qin, C., Gou, Y., Wang, Y., Mao, Y., Liao, H., Wang, Q., et al., 2021. Gas–particle partitioning of polyol tracers at a suburban site in Nanjing, east China: increased partitioning to the particle phase. Atmos. Chem. Phys. 21 (15), 12141–12153.
Qin, Y., Qin, J., Zhou, X., Yang, Y., Chen, R., Tan, J., et al., 2022. Effects of pH on light absorption properties of water-soluble organic compounds in particulate matter emitted from typical emission sources. J. Hazard. Mater. 424, 127688.
Rogge, W.F., Hildemann, L.M., Mazurek, M.A., Cass, G.R., Simoneit, B.R.T., 1993a. Sources of fine organic aerosol .3. Road dust, tire debris, and organometallic brake lining dust - roads as sources and sinks. Environ. Sci. Technol. 27 (9), 1892–1904.
Rogge, W.F., Hildemann, L.M., Mazurek, M.A., Cass, G.R., Simoneit, B.R.T., 1993b. Sources of fine organic aerosol .4. Particulate abrasion products from leaf surfaces of urban plants. Environ. Sci. Technol. 27 (13), 2700–2711.
Shi, G., Xu, J., Peng, X., Xiao, Z., Chen, K., Tian, Y., et al., 2017. pH of aerosols in a polluted atmosphere: source contributions to highly acidic aerosol. Environ. Sci. Technol. 51 (8), 4289–4296.
Shiraiwa, M., Ueda, K., Pozzer, A., Lammel, G., Kampf, C.J., Fushimi, A., et al., 2017. Aerosol health effects from molecular to global scales. Environ. Sci. Technol. 51 (23), 13545–13567.
Shrivastava, M.K., Subramanian, R., Rogge, W.F., Robinson, A.L., 2007. Sources of organic aerosol: positive matrix factorization of molecular marker data and comparison of results from different source apportionment models. Atmos. Environ. 41 (40), 9353–9369.
Simoneit, B.R.T., Elias, V.O., Kobayashi, M., Kawamura, K., Rushdi, A.I., Medeiros, P.M., et al., 2004. Sugars - dominant water-soluble organic compounds in soils and characterization as tracers in atmospheric particulate matter. Environ. Sci. Technol. 38 (22), 5939–5949.
Stangl, C.M., Johnston, M.V., 2017. Aqueous reaction of dicarbonyls with ammonia as a potential source of organic nitrogen in airborne nanoparticles. J. Phys. Chem. A 121 (19), 3720–3727.
Surratt, J.D., Chan, A.W.H., Eddingsaas, N.C., Chan, M., Loza, C.L., Kwan, A.J., et al., 2010. Reactive intermediates revealed in secondary organic aerosol formation from isoprene. Proc. Natl. Acad. Sci. 107 (15), 6640–6645.
Tao, J., Zhang, L., Cao, J., Zhang, R., 2017. A review of current knowledge concerning PM2. 5 chemical composition, aerosol optical properties and their relationships across China. Atmos. Chem. Phys. 17 (15), 9485–9518.
Tian, S.L., Pan, Y.P., Wang, Y.S., 2016. Size-resolved source apportionment of particulate matter in urban Beijing during haze and non-haze episodes. Atmos. Chem. Phys. 16 (1), 1–19.
Tsagkaraki, M., Theodosi, C., Grivas, G., Vargiakaki, E., Sciare, J., Savvides, C., et al., 2021. Spatiotemporal variability and sources of aerosol water-soluble organic nitrogen (WSON), in the Eastern Mediterranean. Atmos. Environ. 246, 118144.
Updyke, K.M., Nguyen, T.B., Nizkorodov, S.A., 2012. Formation of brown carbon via reactions of ammonia with secondary organic aerosols from biogenic and anthropogenic precursors. Atmos. Environ. 63, 22–31.
Verma, S.K., Kawamura, K., Chen, J., Fu, P., 2018. Thirteen years of observations on primary sugars and sugar alcohols over remote Chichijima Island in the western North Pacific. Atmos. Chem. Phys. 18 (1), 81–101.
Violaki, K., Mihalopoulos, N., 2010. Water-soluble organic nitrogen (WSON) in size-segregated atmospheric particles over the Eastern Mediterranean. Atmos. Environ. 44 (35), 4339–4345.
Wang, G., Kawamura, K., Xie, M., Hu, S., Gao, S., Cao, J., et al., 2009. Size-distributions of n-alkanes, PAHs and hopanes and their sources in the urban, mountain and marine atmospheres over East Asia. Atmos. Chem. Phys. 9 (22), 8869–8882.
Wang, G., Li, J., Cheng, C., Hu, S., Xie, M., Gao, S., et al., 2011. Observation of atmospheric aerosols at Mt. Hua and Mt. Tai in central and east China during spring 2009 – Part 1: EC, OC and inorganic ions. Atmos. Chem. Phys. 11 (9), 4221–4235.
Wang, G.H., Li, J.J., Cheng, C.L., Zhou, B.H., Xie, M.J., Hu, S.Y., et al., 2012. Observation of atmospheric aerosols at Mt. Hua and Mt. Tai in central and east China during spring 2009 – Part 2: impact of dust storm on organic aerosol composition and size distribution. Atmos. Chem. Phys. 12 (9), 4065–4080.
Wang, M., Qin, W., Chen, W., Zhang, L., Zhang, Y., Zhang, X., et al., 2020. Seasonal variability of VOCs in Nanjing, Yangtze River delta: implications for emission sources and photochemistry. Atmos. Environ. 223, 117254.
Wang, T., Liu, Y., Cheng, H., Wang, Z., Fu, H., Chen, J., et al., 2022. Significant formation of sulfate aerosols contributed by the heterogeneous drivers of dust surface. Atmos. Chem. Phys. 22 (20), 13467–13493.
Wong, Y.K., Liu, K.M., Yeung, C., Leung, K.K.M., Yu, J.Z., 2022. Measurement report: characterization and source apportionment of coarse particulate matter in Hong Kong: insights into the constituents of unidentified mass and source

origins in a coastal city in southern China. Atmos. Chem. Phys. 22 (7), 5017–5031.
Wu, C., Wang, G., Li, J., Li, J., Cao, C., Ge, S., et al., 2020a. The characteristics of atmospheric brown carbon in Xi'an, inland China: sources, size distributions and optical properties. Atmos. Chem. Phys. 20 (4), 2017–2030.
Wu, C., Zhang, S., Wang, G., Lv, S., Li, D., Liu, L., et al., 2020b. Efficient heterogeneous formation of ammonium nitrate on the saline mineral particle surface in the atmosphere of east Asia during dust storm periods. Environ. Sci. Technol. 54 (24), 15622–15630.
Xie, M., Feng, W., He, S., Wang, Q.g., 2022a. Seasonal variations, temperature dependence, and sources of size-resolved PM components in Nanjing, east. China. J. Environ. Sci. 121, 175–186.
Xie, M., Lu, X., Ding, F., Cui, W., Zhang, Y., Feng, W., 2022b. Evaluating the influence of constant source profile presumption on PMF analysis of PM2.5 by comparing long- and short-term hourly observation-based modeling. Environ. Pollut. 314, 120273.
Xie, M., Peng, X., Shang, Y., Yang, L., Zhang, Y., Wang, Y., et al., 2022c. Collocated measurements of light-absorbing organic carbon in PM2.5: observation uncertainty and organic tracer-based source apportionment. J. Geophys. Res. Atmos. 127 (5), e2021JD035874.
Xu, Y., Miyazaki, Y., Tachibana, E., Sato, K., Ramasamy, S., Mochizuki, T., et al., 2020. Aerosol liquid water promotes the formation of water-soluble organic nitrogen in submicrometer aerosols in a suburban forest. Environ. Sci. Technol. 54 (3), 1406–1414.
Yang, L., Shang, Y., Hannigan, M.P., Zhu, R., Wang, Q.g., Qin, C., et al., 2021. Collocated speciation of $PM_{2.5}$ using tandem quartz filters in northern Nanjing, China: sampling artifacts and measurement uncertainty. Atmos. Environ. 246, 118066.
Yttri, K.E., Dye, C., Kiss, G., 2007. Ambient aerosol concentrations of sugars and sugar-alcohols at four different sites in Norway. Atmos. Chem. Phys. 7 (16), 4267–4279.
Yu, Y., Ding, F., Mu, Y., Xie, M., Wang, Q.g., 2020. High time-resolved $PM_{2.5}$ composition and sources at an urban site in Yangtze River Delta, China after the implementation of the APPCAP. Chemosphere 261, 127746.
Yuan, W., Huang, R.J., Yang, L., Guo, J., Chen, Z., Duan, J., et al., 2020. Characterization of the light-absorbing properties, chromophore composition and sources of brown carbon aerosol in Xi'an, northwestern China. Atmos. Chem. Phys. 20 (8), 5129–5144.
Zhang, Q., Zheng, Y., Tong, D., Shao, M., Wang, S., Zhang, Y., et al., 2019. Drivers of improved $PM_{2.5}$ air quality in China from 2013 to 2017. Proc. Natl. Acad. Sci. 116 (49), 24463–24469.
Zhou, D., Ding, K., Huang, X., Liu, L., Liu, Q., Xu, Z., et al., 2018. Transport, mixing and feedback of dust, biomass burning and anthropogenic pollutants in eastern Asia: a case study. Atmos. Chem. Phys. 18 (22), 16345–16361.